Current Research in Food Science 9 (2024) 100819

Contents lists available at ScienceDirect

Current Research in Food Science

journal homepage: www.sciencedirect.com/journal/current-research-in-food-science

Effect of drying temperature on composition of edible mushrooms: Characterization and assessment via HS-GC-MS and IR spectral based volatile profiling and chemometrics

Chuanmao Zheng [a,b], Jieqing Li [a], Honggao Liu [c,**], Yuanzhong Wang [b,*]

[a] College of Agronomy and Biotechnology, Yunnan Agricultural University, Kunming, 650201, China
[b] Medicinal Plants Research Institute, Yunnan Academy of Agricultural Sciences, Kunming 650200, China
[c] Yunnan Key Laboratory of Gastrodia and Fungi Symbiotic Biology, Zhaotong University, Zhaotong, 657000, Yunnan, China

ARTICLE INFO

Keywords:
Boletus bainiugan
HS-SPME-GC-MS
VOCs
2DCOS
Chemometrics
Quality estimation

ABSTRACT

Edible wild mushrooms are one of the popular ingredients due to their high quality and unique flavor and nutrients. To gain insight into the effect of drying temperature on its composition, 86 *Boletus bainiugan* were divided into 5 groups and dried at different temperatures. Headspace solid-phase microextraction-gas chromatography-mass spectrometry (HS-SPME-GC-MS) was used for the identification of volatile organic compounds (VOCs) of *Boletus bainiugan*. The 21 differential VOCs that distinguish different drying temperatures of *Boletus bainiugan* were identified. 65 °C retained more VOCs. There were differences in their types and content at different temperatures, proteins, polysaccharides, crude fibers, and fats. Fourier transform near-infrared (FT-NIR) spectroscopy, Fourier transform infrared (FTIR) spectroscopy, and two-dimensional correlation spectroscopy (2DCOS) images were successfully characterized for differences in the chemical composition of *Boletus bainiugan*. Partial least squares discriminant analysis (PLS-DA) verified the variability in the chemical composition of *Boletus bainiugan* with the coefficient of determination (R^2) = 0.95 and predictive performance (Q^2) = 0.75 with 92.31% accuracy. Next, infrared spectroscopy provides a fast and efficient assessment of the content of *Boletus bainiugan* nutrients (proteins, polysaccharides, crude fibers, and fats).

1. Introduction

Mushrooms are rich in proteins, polysaccharides, fibers, and other nutrients and are one of the favorite ingredients (Zheng et al., 2023b). Undeniably, they also contribute to good health with mushroom polysaccharides, phenolics, terpenoids, and other bioactive components (Kushairi et al., 2020). Around the world, wild edible mushrooms are more popular, but fewer wild edible mushrooms are available. Fresh mushrooms are perishable food items that tend to lose their quality immediately after harvest (Zhang et al., 2018). Meanwhile, wild mushrooms are affected by climate and the yield is seasonally dependent. Extending the shelf life of mushrooms is an essential challenge, and drying is one of the most widely used methods.

Volatile organic compounds (VOCs) are one of the pivotal factors in determining food quality and consumer selectivity (Deng et al., 2023). Nutrients are contributors to nutritional and medicinal values, and the effect of drying temperature on them cannot be omitted.Headspace solid-phase microextraction (HS-SPME) techniques are often used to extract volatile components with the advantage of rapidity (Gan et al., 2024). Headspace solid-phase microextraction-gas chromatography-mass spectrometry (HS-SPME-GC-MS) is a viable strategy for the comprehensive characterization of sample VOCs (Xie et al., 2023). Tian et al. (2022) identified 51 and 69 VOCs in *Phlebopus portentosus* and *Cantharellus yunnanensis*, respectively, using HS-SPME extraction technique. Drying at 50–60 °C was more effective for total phenol retention than at higher temperatures (Zheng et al., 2021). Aldehydes, ketones, and volatile sulfur-containing compounds are the main aroma substances of mushrooms, and drying at 30–50 °C favors their retention (Lu et al., 2022). Consequently, the effect of drying temperature on mushroom VOCs and quality is of interest to consumers. *Boletus bainiugan* are a popular ingredient. Efforts and data on comparative studies on VOCs of *Boletus bainiugan* at different temperatures are

* Corresponding author.
** Corresponding author.
E-mail addresses: honggaoliu@126.com (H. Liu), boletus@126.com (Y. Wang).

https://doi.org/10.1016/j.crfs.2024.100819
Received 11 June 2024; Received in revised form 15 July 2024; Accepted 10 August 2024
Available online 11 August 2024

limited.

Alternatively, spectroscopic techniques have the advantage of non-destructive, rapid analysis. Spectral analysis has shown that Fourier transform near-infrared (FT-NIR) spectroscopy is the principal instrument for combinatorial and octave information of molecular vibrations, such as C-H, O-H, N-H, and other hydrogen-containing groups in organic matter (Badaró et al., 2022). Other structural information is generally not characterized in this wavelength range, whereas Fourier transform infrared (FTIR) spectroscopy can detect the chemical composition of the object to be measured and related compounds, with energy provided by molecular bonding motions (vibrations) (Zhang and Wang, 2023a). Two-dimensional correlation spectroscopy (2DCOS) can be used to characterize the molecular changes in *Boletus bainiugan* for the influence of temperature. 2DCOS provides finer information by increasing the resolution of infrared (IR) spectroscopy (Lin et al., 2023).

Based on the effect of processing on the nutrient composition of *Boletus bainiugan*, it is a necessary to provide a rapid and effective assessment method. It is common to rapidly rely on infrared spectroscopy and chemometric methods to evaluate substrate quality. Partial least squares regression (PLSR) can find the relationship between the X variable (spectral data) and the Y variable (content data) to build a mathematical model. Cruz-Tirado et al. (2023) predicted protein and lipid content in black soldier fly (*Hermetia illucens* L.) larvae flour using portable near-infrared spectroscopy and PLSR. Yan et al. (2023) predicted the content of uridine, guanosine and adenosine in *Lanmaoa asiatica* based on FT-NIR spectroscopy combined with PLSR method.

Few studies have reported differences in the VOCs and nutrient composition of *Boletus bainiugan* at different drying temperatures. It should be noted that there are no characterization studies on differences in the chemical composition of *Boletus bainiugan* based on HS-SPME-GC-MS, IR spectroscopy, and rapid assessment of nutrient content. Thus, our objective was to analyze the effect of temperature on VOCs and nutrient composition of *Boletus bainiugan* to enable characterization of chemical composition and rapid assessment of nutrient content. To provide a reference for the study of the effect of temperature on the nutrient and aroma components of mushrooms.

The present study was carried out with different drying temperature gradients (35 °C, 45 °C, 55 °C, 65 °C, and 75 °C) of *Boletus bainiugan* outside the study material. HS-SPME-GC-MS was selected to analyze their VOCs and to screen for differential compounds affected by temperature. Additionally, their proteins, polysaccharides, crude fibres and fats content were determined. Subsequently, the chemical composition was characterized using FT-NIR, FTIR, and 2DCOS images.The differences in chemical composition of *Boletus bainiugan* at different temperatures were examined using PLS-DA. It also provides an analytical method for rapid estimation of quality food ingredients (high nutrient content), based on the combination of IR spectroscopy and nutrient content to build a PLSR model.

2. Materials and methods

2.1. Materials

A total of 86 *Boletus bainiugans* from Kunming, Yunnan, China were dried at constant temperatures at five temperatures, 35 °C (17), 45 °C (16), 55 °C (18), 65 °C (18), and 75 °C (17) (Table S1). Three samples were mixed at each of the five temperatures for the HS-SPME-GC-MS analysis of volatile components. Additionally, to improve the performance of the model and to make the samples more representative of the reality of the market, we purchased 71 samples with known drying temperatures from the Mushuhua market in Yunnan, China (Table S1). All samples were pulverized, passed through a 100 mesh sieve, and then sealed and stored at room temperature.

2.2. Chemical reagents

NaCl (Sinopharm Chemical Reagent Co., Ltd, Shanghai, China), Hexyl hydride (Merck, Shanghai, China), Standard products (p-Xylene-d10) (BioBioPha/Sigma-Aldrich, Shanghai, China). Other reagents, including $CuSO_4 \cdot 5H_2O$, K_2SO_4, H_2SO_4, H_3BO_3, NaOH, C_2H_5OH of 95%, KOH.

2.3. HS-SPME-GC-MS conditions

(1) Weigh approximately 0.2 g (0.2 ml liquid) of each sample in a headspace vial; (2) add 0.2 g of NaCl powder and 20 μL (10 μg/mL) of the internal standard solution; (3) extract the samples by fully automated HS-SPME and analyze by GC-MS.

After sampling, the desorption of the VOCs from the fiber coating was carried out in the injection port of the GC apparatus (Model 8890; Agilent) at 250 °C for 5 min in the splitless mode. Identification and quantification of VOCs were carried out using an Agilent Model 8890 GC and a 7000D mass spectrometer (Agilent), equipped with a 30 m × 0.25 mm × 0.25 μm DB-5MS (5% phenyl-polymethylsiloxane) capillary column. Helium was used as the carrier gas at a 1.2 mL/min linear velocity. The injector temperature was kept at 250 °C. The oven temperature was programmed from 40 °C (3.5 min), increasing at 10 °C/min to 100 °C, at 7 °C/min to 180 °C, at 25 °C/min to 280 °C, and held for 5 min. Mass spectra were recorded in electron impact (EI) ionization mode at 70 eV. The quadrupole mass detector, ion source, and transfer line temperatures were set, respectively, at 150, 230 and 280 °C. The MS was selected ion monitoring (SIM) mode was used to identify and quantify analytes.

2.4. Determination of proteins, polysaccharides, crude fibers, and fats

157 samples of *Boletus bainiugan* were determined for protein, polysaccharides, crude fibers, and fats (Metware Biotechnology Co. Wuhan, China).

2.4.1. Proteins

The determination was carried out according to GB 5009.5–2016 "National Standard for the Food Safety Determination of Proteins in Food", the first method is the Kjeldahl method. The principle is that the proteins in the food are broken down under catalytic heating conditions and the resulting ammonia combines with sulphuric acid to form ammonium sulphate. Alkaline distillation frees ammonia, which is absorbed with boric acid and then titrated with a standard titration solution of sulphuric or hydrochloric acid, and the nitrogen content is calculated from the consumption of the acid and multiplied by a conversion factor to give the protein content (Archibald et al., 1958). For protein content $\geq$1 g/100 g, the results are retained to three significant figures; for protein content <1 g/100 g, the results are retained to two significant figures.

2.4.2. Polysaccharides

The total polysaccharides were extracted using aqueous alcohol precipitation method, and the total polysaccharide content was determined by phenol-sulphuric acid method (Sun et al., 2023). (i). Dry and grind the sample through a 40-mesh sieve, weigh 5 mg of sieved powder into a 2 mLEP tube, add 1 mL of distilled water; heat in a boiling water bath (95–100 °C) for 2 h (seal the film tightly to prevent water loss); cool to room temperature, centrifuge at 8000 rpm for 5 min, and take the supernatant. (ii). Take 0.2 mL of supernatant into a new EP tube, add 0.8 mL of Reagent 2 and mix well, let it stand at 4 °C overnight; after removing it, centrifuge at 8000 rpm for 5 min, discard the supernatant and leave the precipitate (try to keep the precipitate as much as possible); (iii). Add 1 mL of distilled water to the precipitate obtained in the previous step, mix thoroughly to dissolve the precipitate, and leave it for measurement.

2.4.3. Crude fibers

The crude fibers content was determined according to the standard of GB/T 5009.10–2003 (Ma et al., 2021). (i). Weigh 20 g–30 g of mashed specimen (or 5.0 g in specimen), transfer to a 500 mL conical flask, add 200 mL of boiled 1.25% sulphuric acid, heat to bring to a slight boil, keep the volume constant, and maintain for 30 min, shake the conical flask every 5 min to mix the substances in the flask sufficiently. (ii). Remove the conical flask and immediately filter it through a linen cloth and wash it with boiling water until the washings are not acidic. (iii). Then use 200 mL of boiling 1.25% potassium hydroxide solution; the linen on the residue washed into the original conical flask heated to a slight boil for 30 min after removing the conical flask, immediately filtered through linen; washed with boiling water for 2 to 3 times, transferred to the dry and weighed G2 pendant melting crucible or the same type of pendant melting funnel, filtration, washed with hot water after sufficiently, drained. Wash with ethanol and ether once more. Dry the crucible and contents in an oven at 105 °C and weigh, repeat until a constant quantity is obtained.

2.4.4. Fats

The fats content was determined according to the GB/5009.6–2016 National Standard for Food Safety Determination of Fats in Foods (Nielsen and Carpenter, 2017), the first method: Soxhlet extraction method. The principle is: fat is soluble in organic solvents. The sample is extracted directly with anhydrous ether or petroleum ether and other solvents, then the solvent is removed by evaporation and dried to obtain the free fat content.

2.5. Infrared spectra collection

A total of 157 samples were acquired with FT-NIR and FTIR spectra. FT-NIR spectra were collected in the spectral range of 10,000–4000 cm^{-1} using the instrument Antaris II FT-NIR spectrometer (Thermo Fisher Scientific INC., USA). The acquisition mode was diffuse reflection mode, and the background was acquired at 64 min intervals. The resolution was 8 cm^{-1} and the acquisition parameter was 64 times, with two repetitions per sample, and the final average spectrum was selected (Yan et al., 2023).

FTIR was acquired using an FTIR spectrometer (Thermo Fisher Scientific, USA) equipped with a single-point diamond attenuated total reflection (ATR) attachment and OMNIC 9.77 software. The acquisition range was 4000-400 cm^{-1} with 16 scans per spectral stack and a resolution of 8 cm^{-1}, and the scans were repeated three times to obtain an average IR spectrum. Background acquisitions were made at 30-min intervals to eliminate the effects of atmospheric H_2O and CO_2.

2.6. HS-SPME-GC-MS data processing

The raw data downstream after mass spectrometry analysis were processed by MassHunter software for qualitative and quantitative analysis. Volatile metabolite profiling was performed using Metware Cloud, a free online platform for data analysis (https://cloud.metware.cn).

A principal component analysis (PCA) was performed on the samples, including quality control samples, to understand the general differences in metabolites between samples groups and the magnitude of variability between samples within groups (Ye et al., 2024). The PCA results showed a trend of separation of metabolites between groups, suggesting whether or not the metabolites differed within the samples group (Chen et al., 2009). PCA was performed with the built-in statistical prcomp function of the R software (www.r-project.org/), and the prcomp function parameter scale = True was set to indicate the UV (unit variance scaling) processing of the data.

Orthogonal partial least squares discriminant analysis (OPLS-DA) combines orthogonal signal correction (OSC) and PLS-DA methods, which can decompose the X matrix information into two categories of information related and uncorrelated with Y, and filter the difference variables by removing the uncorrelated differences (Esteves et al., 2022). OPLS-DA is centered after the raw data are log2 transformed. Where X is the sample quantitative information matrix and Y is the sample grouping information matrix. The analysis was then performed using the MetaboAnalystR package OPLSR. Anal function in R software. Volcano graphs and Venn diagram analysis of the number of differential metabolites are based on online tools (https://cloud.metware.cn).

The predictive parameters of the OPLS-DA evaluation model are R^2X, R^2Y, and Q^2, where R^2X and R^2Y denote the explanatory rate of the constructed model on the X and Y matrices, respectively, and Q^2 denotes the predictive capacity of the model, and the closer the three indexes are to 1 means that the model is more stable and reliable, and the model can be regarded as a valid model when $Q^2 > 0.5$, and an excellent model when $Q^2 > 0.9$ (Zhong et al., 2024). The model was used to perform 200 random permutation experiments on the data. In general, the model was best when $p < 0.05$.

We selected differential metabolites based on VIP≥1, fold change≥2 or ≤2, and $p < 0.05$. Their odour flavour analyzes were performed via the website (http://www.thegoodscentscompany.com, http://perflavory.com/, http://www.odour.org.uk/odour/index.html,http://foodflavorlab.cn/#/home).

2.7. Spectral data analytics

2.7.1. Preprocessing

Spectral acquisition faces problems such as baseline shift, noise, and scattering effects due to the effect of optical range variation and sample particle size, so preprocessing is very necessary (Badaró et al., 2022). SIMCA (14.1 Umetrics, Sweden) software was selected for the study for pre-processing. Standard normal variable transform (SNV) and multivariate scattering correction (MSC) can reduce the scattering effect in spectral data. The derivative and Savitzky-Golay (SG) smoothing improves spectral resolution and reduces noise (Zhang and Wang, 2023b).

2.7.2. Two-dimensional correlation spectral analysis

The 2DCOS analysis was used to characterize the changes in the chemical composition of *Boletus bainiugan* at different drying temperatures, and a one-dimensional spectrum was selected for 2DCOS analysis at each temperature using temperature as external interference (Lin et al., 2023). The FTIR spectra were segmented into functional group region (3600-2500 cm^{-1}) and fingerprint region (1650-400 cm^{-1}) to enhance the clarity of the spectral peaks, and synchronized 2DCOS was generated based on the calculation of the discrete Hilbert transform algorithm. It was generated by the Matlab software (R2017b. MathWorks, USA) to run scripts (Dong et al., 2022). The column vector f denotes the dynamic spectral intensity (Eq. (1)) when the spectra are measured in n-step equal time intervals.

$$f(i) = \begin{cases} f(i,t1) \\ f(i,t2) \\ \vdots \\ f(i,tn) \end{cases} \quad (1)$$

The strength of the simultaneous two-dimensional correlation between variables i1 and i2 is expressed as (Eq. (2)):

$$\varphi(i1,i2) = \frac{1}{m\text{-}1} f(i1)^{T}.f(i2) \quad (2)$$

Where: φ (i1, i2) denotes the synchronized 2DCOS, m is the number of spectra, and the data matrix f consists of the average spectrum and the ith spectrum at each sampling point.

2.7.3. Principal component analysis

PCA makes the samples relatively clustered in a certain area, reflecting the similarity and difference between them, in the case of retaining more original information. It uses the information between

samples to visualize the trend of sample distribution and has the purpose of feature extraction and dimensionality reduction (Zhang and Wang, 2023b).

2.7.4. Partial least squares-discriminant analysis

SIMCA software (14.1 Umetrics, Sweden) was provided to build the PLS-DA model. It serves as a supervised identification method, PLS-DA was used for the identification of the drying temperature of porcini mushrooms with the role of testing the variability of the samples (He et al., 2023). Based on Latent variables (LVs), the Coefficient of determination (R^2); Indicates the prediction ability of the model to new data (Q^2); the root mean square error of estimation (RMSEE); Root mean square error of cross-validation (RMSEcv); Root mean square error of prediction (RMSEP) and accuracy to assess the model performance. R^2, Q^2, and accuracy are close to 1 while RMSEE, RMSEcv, and RMSEP are close to 0, so the model performance is superior (Zheng et al., 2023a).

2.7.5. Partial least squares regression analysis

The PLSR model finds the best linear correlation between the independent matrix X (spectra) and the measured parameter Y (content) of the sample (Yan et al., 2023). It was built on the basis of FTIR spectra and content (protein, polysaccharide, crude fiber, fat) in the software The Unscrambler X 10.4. Based on the parameters latent variables (LVs); calibration set coefficient of determination (R^2c); prediction set coefficient of determination (R^2p); calibration set root mean square error (RMSEC); prediction set root mean square error (RMSEP) and Bias to evaluate the model performance. For good models, R^2c and R^2p are close to 1, RMSEC close to 0, RMSEP, and Bias are very necessary (Peng et al., 2024).

3. Results

3.1. Differences in VOCs at different temperatures

3.1.1. HS-SPME-GC-MS metabolic profiles of Boletus bainiugan

To verify that temperature affects the chemical compositional homeostasis of *Boletus bainiugan*, non-targeted metabolomics provided a comprehensive and systematic examination of metabolites at a holistic level. VOCs from *Boletus bainiugan* treated with different drying temperatures were analyzed by HS-SPME-GC-MS, and a total of 764 metabolites were detected (Supplementary Material 1). Includingacid (11), alcohol (52), aldehyde (46) and amine (20), aromatics (43) and ester (129), halogenated hydrocarbons (4), heterocyclic compound (123). hydrocarbons(75), ketone(47), nitrogen compounds(7), others (5), phenol(17), sulfur compounds(6), terpenoids(180). Among them, terpenoids, ester, and heterocyclic compounds were the major volatiles, accounting for 23.53%, 16.21%, and 16.08% of the total volatiles, respectively (Fig. 1a). 737 compositions were measured at 35 °C, 709 at 45 °C, 735 at 55 °C, 737 at 65 °C, and 75 °C had 748 components. Of these, 55 components were not detected at 45 °C, containing the most esters with 15, heterocycles with 14, and terpenes with 9.

The volatile compounds of *Boletus bainiugan* changed significantly at different temperatures (Fig. 1b). It was straightforwardly observed that the major contributing components included Alcohol, Aldehyde, Aromatics, Ketone, and Terpenoids. Overall, all categories, except for Others and Sulfur compounds, were consistently highest at D (65 °C) (Fig. 1b). The Alcohol content of A (35 °C) and C (55 °C) were significantly different ($p < 0.05$), with 55 °C having the highest Alcohol content. Besides, there was no significant difference ($p > 0.05$) in Alcohol content in B (45 °C), 65 °C, and E (75 °C). Fig. S1 provides a heat map of the clustering of VOCs of *Boletus bainiugan* at different drying temperatures, as well as clustering analysis of 65 °C versus other temperatures. The cluster analysis shows that 65 °C and 45 °C are clustered into 1 class, indicating that their chemical compositions are similar. Next, the overall chemical composition content of 65 °C is higher than the other temperatures.

3.1.2. Multivariate data analysis

Before analyzing variance, it is the magnitude of variability between the subgroups of the observed differences and between the samples within the group, by performing a principal component analysis of the subgroup samples for comparison of differences. The stability and reliability of the method were allowed due to the PCA results that group the quality control (QC) samples together (Fig. 1c). Together, PC1 and PC2 explained 51.50% of the variance. The PCA score plot showed a clear clustering trend, illustrating the high variance in the volatile components of *Boletus bainiugan* based on different drying temperatures. Positive scores were observed in the PC1 direction at 45 °C and 65 °C,

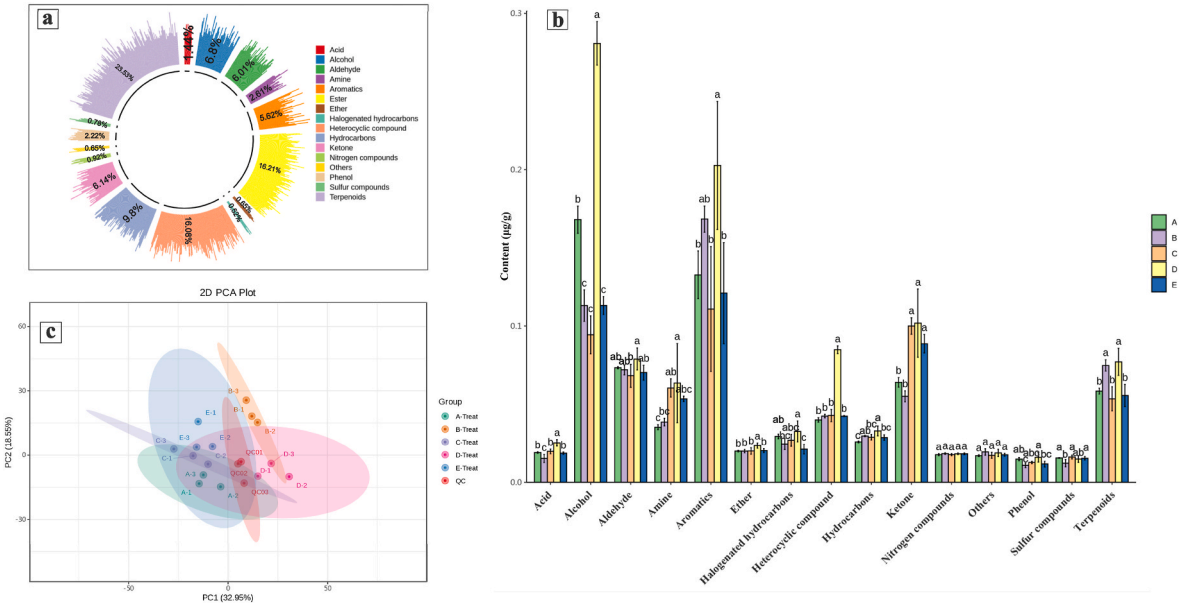

Fig. 1. Trends in volatile substances. (a) Proportion of various volatile compounds in *Boletus bainiugan*. (b) Content of volatile substances at different drying temperatures. Different letters for the same volatile category indicate significant differences at the $p < 0.05$. (c) Score plot of principal component analysis of volatile substances. (A) 35 °C, (B) 45 °C, (C) 55 °C, (D) 65 °C, (E) 75 °C.

respectively, while negative scores were observed at 35 °C, 55 °C and 75 °C, respectively. This could be the resultof the volatile component content, as the difference in terpenoid content was significant in *Boletus bainiugan* dried at 45 °C and 65 °C (maximum percentage of 23.53%) as compared to the other components.

PCA is insensitive to less relevant variables, which OPLS-DA can address. Therefore, a two-by-two comparison of 65 °C with others was performed for OPLS-DA analysis to elucidate better the difference between 65 °C and other drying temperatures. Model performance was excellent, with both R^2 and Q^2 close to 1. Model parameters are listed in Table S2. As shown in Figs. S2 and 65°C showed excellent clustering compared to other two-by-two comparisons. Also, a permutation test (n = 200) was used with $p < 0.05$, which does not produce overfitting (Fig. S3). Thus OPLS-DA models can differentiate *Boletus bainiugan* with different drying temperatures based on differences in chemical composition.

So next, differential metabolites were identified in *Boletus bainiugan* at different drying temperatures, using VIP≥1, fold change≥2 or ≤2, and $p < 0.05$ as the criteria (Zhang et al., 2020). 46 differential metabolites were identified (36 up-regulated and 10 down-regulated) between 65 °C and 35 °C, 46 differential metabolites (45 up-regulated and 9 down-regulated) between 65 °C and 45 °C, 44 differential metabolites were identified between 65 °C and 45 °C (45 up-regulated and 9 down-regulated), 88 differential metabolites were identified between 65 °C and 55 °C (84 up-regulated and 4 down-regulated), and 62 differential metabolites were identified between 65 °C and 75 °C (6 up-regulated and 56 down-regulated) (Fig. S4). A total of 21 volatile differential metabolites were identified among *Boletus bainiugan* with different drying temperatures (Fig. S4e, Table S3). It included eight classes of substances: Alcohol, Ester, Heterocyclic compound, Hydrocarbons, Ketone, Nitrogen compounds, Phenol, and Terpenoids.

3.2. Spectral characterization

3.2.1. Spectral characterization of the chemical constituents of Boletus bainiugan

The temperature affected the molecular structure of the chemical composition of *Boletus bainiugan* (Table 1). The FT-NIR spectral profile and 2DCOS images are provided in Fig. 2. The second overtone of C-H stretching (HC=CH) resulted in absorption peaks of 8527.68–8246.12 cm^{-1} spectral bandwidth. The absorption band of 6927.05–6186.52 cm^{-1} was caused by the absorption of the first overtone of the O-H stretching vibration and the third overtone of the C-O stretching vibration. The absorption peak in the 5920.39–5619.55 cm^{-1} band is attributed to the first overtone of C-H stretching and CH_2 symmetry vibration. A narrower absorption peak appears in the 5233.86–5060.3 cm^{-1} spectral band associated with O-H stretching and H-O-H bending vibrations. The absorption peaks in the 4747.88–4520.33 cm^{-1} band are associated with O-H, C-O, and C=O-O stretching vibrations. The other absorption peak appears in the range 4385.33–4231.06 cm^{-1} and is caused by the second overtone of the C-H and C-H_2 bending vibrations (Drees et al., 2023). From Fig. 3a, it can be seen that the absorption intensity of the FT-NIR spectra is related to the drying temperature. In this case 3600-2500 cm^{-1}, the spectral absorption intensity has 45 °C > 35 °C > 75 °C > 55 °C > 65 °C (Fig. 3b). Also, 1650-400 cm^{-1} has a similar phenomenon (Fig. 3c).

The FTIR spectra of *Boletus bainiugan* are shown in Fig. 3. Two strong absorption peaks appear in the spectral band 3600-2500 cm^{-1}, near 3266.82 which are principally produced by the OH vibrations of water, alcohols, and phenols; The other absorption peak is near 2925 cm^{-1}, which is attributed to the CH_2 symmetric vibration in unsaturated lipids. There are two narrow accessory peaks near 2874.38 cm^{-1}, which are related to carbohydrates, carboxylic acids, carboxylic acids, and amino acids (Fig. 3b). Another thing that is not difficult to observe is that a minor difference appeared near 1730 cm^{-1} of the spectral band, related to the C=O vibrational bonding of Ester in *Boletus bainiugan* (Fig. 3c).

Table 1
Main fingerprint peaks of *Boletus bainiugan* dried at different temperatures.

Wavenumber (cm^{-1})	Base group and vibration mode	Component	References
8527.68–8246.12	υ (HC=CH)	lipids	Veselá et al. (2007)
6927.05–6186.52	υ (O-H)	carbohydrates, proteins, water	Drees et al. (2023)
5920.39–5619.55	υ (O-H), $υ_s$ (C-H_2)	aliphatic hydrocarbons	Drees et al. (2023)
5233.86–5060.3	υ (O-H), δ(H-O-H)	–	Drees et al. (2023)
4747.88–4520.33	υ (O-H), υ (C-O), υ (C=O-O)	hydrocarbons	Drees et al. (2023)
4385.33–4231.06	δ(O-H), δ(C-H_2)	–	Drees et al. (2023)
3266.82	υ (OH)	water, alcohols, phenols	Surek et al. (2022)
2925	$υ_s$ (CH_2)	unsaturated lipid	Christou et al. (2018)
2874.38	υ (C-H), υ (O-H), υ (NH_3)	Carbohydrates, carboxylic acids, amino acids	Aykas et al. (2023)
2854.13	δ (CH_2)	lipids, proteins	Rohman and Man (2010)
1624.25	υ (COO-), υ (C=O)	protein	
1554.83	υ (C=C)	aromatic rings, alkaloids, flavonoids, acid	(Chen et al., 2018; Jingying et al., 2023; Surek et al., 2022)
1450.58	δ (C-H), υ (aromatic), υ (CH_2), (CH_3)	flavonoids, aromatic ring	Moţ et al. (2011)
1399.1	–	phenolic compounds	Jingying et al. (2023)
1314.25	$υ_{as}$ (-C-N-C-)	aromatic compounds	Choong et al. (2011)
1256.88	$υ_s$ (C-O)	lipids	–
1027.39	υ (C-O)	ester group, secondary alcohol	Mabasa et al. (2021)
617.1	υ (C-H)	alkynes	Vanitha et al. (2019)
525.57	δ (saccharide ring)	polysaccharide	Choong et al. (2011)

Note: υ, stretching mode; δ, bending mode; s, symmetric; and as, asymmetric.

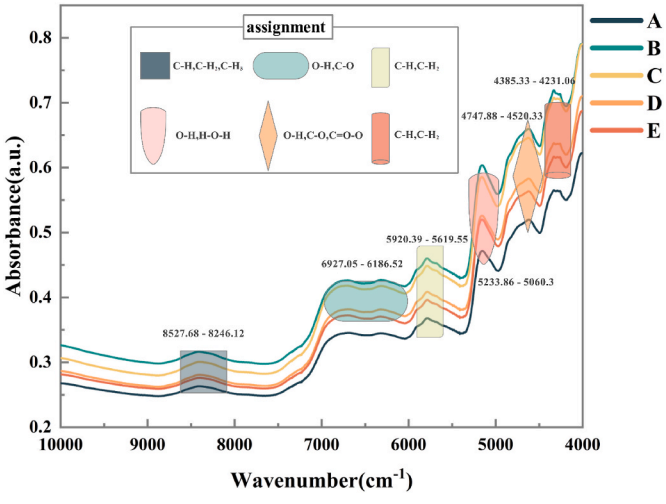

Fig. 2. FT-NIR spectra of *Boletus bainiugan* at five drying temperature gradients. (A) 35 °C, (B) 45 °C, (C) 55 °C, (D) 65 °C, (E) 75 °C.

The spectrogram of this spectral segment shows the highest intensity in treatment B (45 °C), which may be the highest Ester content in *Boletus bainiugan* at 45 °C.

Moving on, the 1650-400 cm^{-1} spectral band can be regarded as a

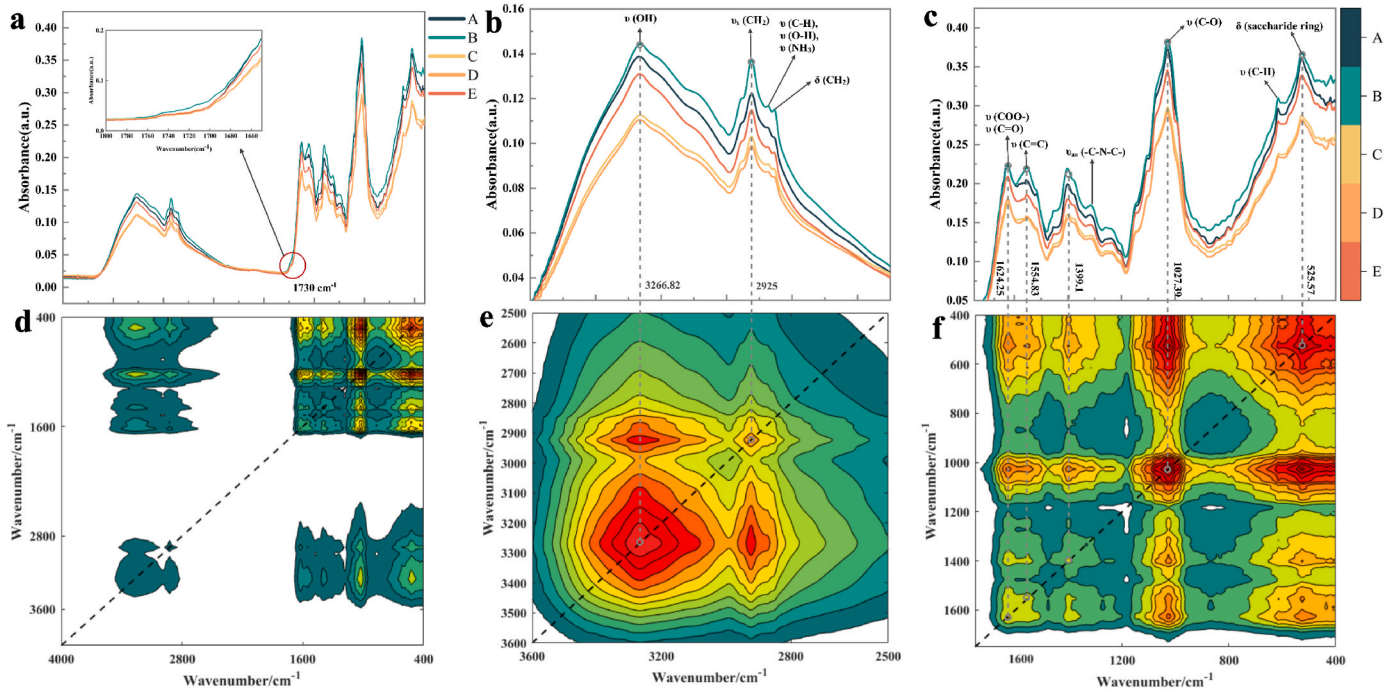

Fig. 3. FTIR spectra with five drying temperature gradients and 2DCOS profiles of *Boletus bainiugan*, (a),(d) full spectrum; (b),(e) 3600-2500 cm^{-1}; (c),(f) 1650-400 cm^{-1}. (A) 35 °C, (B) 45 °C, (C) 55 °C, (D) 65 °C, (E) 75 °C.

characteristic spectral region owing to the inclusion of complex and variable chemical information. Among them, the absorption peak appearing at 1624.25 cm^{-1} is associated with the protein content. The absorption peak near 1554.83 cm^{-1} is elicited by the C=C stretching vibration in aromatic rings, alkaloids, flavonoids, and acids. The absorption peaks near 1450.58 cm^{-1} are assigned to flavonoids, aromatic rings, and phenolic compounds near 1399.1 cm^{-1}. The distinct absorption peak near 1399.1 cm^{-1} and its subsidiary peaks at 1314.25 cm^{-1} and 1256.88 cm^{-1}, respectively, are observed. They are linked to phenolic compounds, aromatic compounds, and lipids, respectively. It is the strongest absorption peak near 1027.39 cm^{-1} ascribed to the C-O stretching vibration of the ester group, secondary alcohol. Stronger absorption peaks also appeared near 525.27 cm^{-1} and it appeared an accessory peak at 617.1 cm^{-1} associated with polysaccharide and alkynes respectively. It must be recognized that the above resolution is only the principal absorption of the spectrum of *Boletus bainiugan*, and its entire spectra are attributed to the complex chemical composition of *Boletus bainiugan*. One-dimensional FTIR spectra are characterized by more overlapping regions and unknown components that are not observed by the analysis. On the basis of this, the 2DCOS image has high resolution and provides more chemical information.

Fig. 3d shows the simultaneous 2DCOS spectral images of the full spectrum and the principal absorption peaks spectra (3600-2500 cm^{-1}, and 1650-400 cm^{-1}) of *Boletus bainiugan*. The automatic peaks appeared on the diagonal lines of the 2DCOS images, signifying the degree of sensitivity of the correlation spectra in different regions to the change in spectral intensity induced by the perturbation. Synchronized variations of spectral signals at different wavelengths produce cross peaks, located on the off-diagonal lines, indicating that there may be stronger synergism or stronger interactions between the moieties (Lin et al., 2023). The 3600-2500 cm^{-1} spectral band exhibited a strong and broad auto peak (3266.82 cm^{-1}) and a stronger and narrower auto peak (2925 cm^{-1}) associated with the stretching vibration of OH and the bending vibration of CH_2, respectively (Fig. 3e). The 2DCOS image of another characteristic spectral band (1650-400 cm^{-1}) exhibits complex auto peaks and cross peaks (Fig. 3f). There are four regions in this spectrum where strong auto peaks appear near 1624.25 cm^{-1}, 1399.1 cm^{-1}, 1027.39 cm^{-1}, and 525.57 cm^{-1}, which are attributed to protein, phenolic compounds, ester group, and secondary alcohol. Simultaneously, the cross-peaks were formed by synergistic interactions between them. For example, cross-peaks were formed near 1624.25 cm^{-1} and the remaining three wave numbers and the strength was related to the strength of the FTIR spectral pattern. So, the intensity of the cross peak formed at 1624.25 cm^{-1} jointly with 1399.1 cm^{-1} and 525.57 cm^{-1} is higher than that formed at 1027.39 cm^{-1}. Subsequently, it was compared with the 2DCOS images of different temperatures of dried *Boletus bainiugan* at 3600-2500 cm^{-1} and 1650-400 cm^{-1} separately (Fig. S5).

The FTIR spectral information showed that the 2DCOS image profiles were similar at different drying temperatures, but the number and area of the contours were different. This indicated that the chemical composition of *Boletus bainiugan* was similar at different temperatures, but the content and spectral absorption peak intensities varied greatly, showing 35 °C > 45 °C > 75 °C > 55 °C > 65 °C. The effect of drying temperature on the chemical composition of *Boletus bainiugan* was further analyzed in an unsupervised exploratory analysis.

3.2.2. Exploratory analysis

PCA, to visualize the differences between the chemical compositions of *Boletus bainiugan* based on different drying temperatures, an unsupervised pattern recognition method in multivariate statistical analysis was used. It achieves an objective classification of *Boletus bainiugan* with different drying temperatures by downscaling complex data, presenting that different drying temperatures make differences in the chemical composition of *Boletus bainiugan*. Before this Hotelling's T^2 test for outliers was performed to eliminate outliers with a confidence level of more than 95% (FTIR: 5; FT-NIR: 4), and the results are shown in Fig. 4 (a–c). The score graphs, with $R^2X = 0.994$, $Q^2(cum) = 0.991$ (FTIR); $R^2X = 0.996$, $Q^2(cum) = 0.996$ (FT-NIR), indicate that it has better model interpretation and prediction ability.

Fig. 4b shows the differences in chemical composition between the sample points, A (35 °C), B (45 °C), and E (75 °C) have a tendency to overlap, D (65 °C) has another clustering, and C (55 °C) is covered in two clusters. It shows a similar trend with the FTIR spectrogram, which is contributed by the groups of alcohols, phenols, amino acids, lipids,

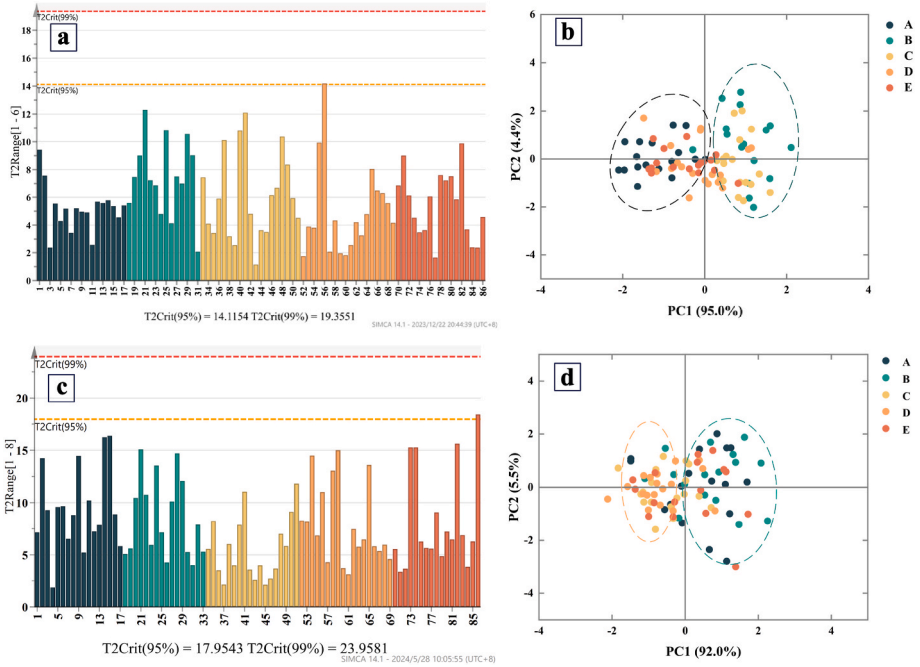

Fig. 4. Detection of Hotelling T^2 outliers and PCA score plots. (a), (b) FT-NIR and (c), (d) FTIR. (A) 35 °C, (B) 45 °C, (C) 55 °C, (D) 65 °C, (E) 75 °C.

proteins, flavonoids, ester, and other substances. Collectively, the drying temperature affected the chemical composition of *Boletus bainiugan*, causing the FT-NIR and FTIR to undergo variability visible to the naked eye.

3.2.3. PLS-DA model to validate chemical compositional variability

FT-NIR, FTIR, and data fusion spectral data were preprocessed to build the PLS-DA model (Table 2). The lowest R^2 and Q^2 were 0.75, 0.57, and greater than 0.5, respectively, indicating good model performance. The highest RMSEE, RMSEcv, and RMSEP were 0.20, 0.29, and 0.28 respectively, and the lowest accuracy was 95.00% and 88.46% for the training set and test set separately. Among the data fusion, both the training set and prediction set accuracies were optimal at 100% and 92.31%, with R^2 and Q^2 reaching 0.95 and 0.74. The modeling results indicated that there was intergroup variability in the chemical composition of *Boletus bainiugan* at different drying temperatures selected in this study and that PLS-DA modeling combined with spectral identification of the processing method (drying temperature) was feasible. The PLS-DA model was built based on FT-NIR, FTIR, and data fusion, and the data fusion showed optimal results. This is related to spectral information, where FT-NIR and FTIR fusion provide more comprehensive chemical information.

3.3. Establishment of rapid quality assessment method for Boletus bainiugan

They are the main nutrients of mushrooms, crude proteins, polysaccharides, fats, and crude fibers, and the effect of temperature is crucial. Table S4 shows the content profiles of the four principal components at five temperatures. There was no significant difference in the content of crude proteins and crude fibers between all treatments; the total fat content was significantly different ($p < 0.05$) between 55 °C and 75 °C; for total polysaccharides, there was no significant difference between 45 °C and 75 °C, for and they were significantly different from other temperatures. Proteins, polysaccharides, crude fibers, and fats are essential for the assessment of the quality of boletes. FTIR mirrors the stretching vibration of functional groups or chemical bonds of chemical components, as well as the bending and carbon skeleton fingerprint vibration, and the variation of chemical components has a specific fingerprint region. Based on this, in this study, FTIR combined with protein, polysaccharide, crude fibers, and fat content was chosen to establish a PLSR model for rapid prediction and evaluation of the quality

Table 2
Differential test of spectrochemical information at different temperatures based on PLS-DA models.

Spectral band/cm^{-1}	Spectral pretreatment	LVs	R^2	Q^2	RMSEE	RMSEcv	RMSEP	Train acc/%	Test acc/%
10,000–4000	SD	7	0.87	0.68	0.15	0.20	0.23	100.00	88.46
	SD-SNV	6	0.78	0.58	0.19	0.25	0.20	95.00	88.46
	SD-MSC	**6**	**0.85**	**0.60**	**0.15**	**0.25**	**0.19**	**98.33**	**92.31**
	SD-MSC-SG	**7**	**0.83**	**0.61**	**0.16**	**0.24**	**0.19**	**98.33**	**92.31**
	SD-SNV-SG	5	0.75	0.57	0.20	0.26	0.21	95.00	88.46
4000–400	**SD-MSC**	**10**	**0.96**	**0.68**	**0.09**	**0.29**	**0.28**	**100.00**	**88.46**
	SD-SNV	**10**	**0.96**	**0.63**	**0.09**	**0.29**	**0.27**	**100.00**	**88.46**
	SD-MSC-SG	10	0.96	0.66	0.10	0.29	0.28	100.00	88.46
	SD-SNV-SG	10	0.96	0.63	0.10	0.29	0.27	100.00	88.46
dataset fusion	**SD-MSC**	**9**	**0.95**	**0.75**	**0.10**	**0.25**	**0.23**	**100.00**	**92.31**
	SD-SNV	**9**	**0.95**	**0.75**	**0.10**	**0.25**	**0.23**	**100.00**	**92.31**
	SD-MSC-SG	**9**	**0.95**	**0.74**	**0.10**	**0.25**	**0.23**	**100.00**	**92.31**
	SD-SNV-SG	**9**	**0.95**	**0.74**	**0.10**	**0.25**	**0.23**	**100.00**	**92.31**

Note: LVs: latent variables; R^2: goodness of fit; Q^2:goodness of prediction; RMSEE: Estimating the root mean square error; RMSEcv: Cross-validation root mean square error; RMSEP: prediction root mean square error; SD: Second derivative; MSC: Multiplicative signal correction; SNV: Standard normal variate; SG: Savitzky-Golay.

of *Boletus bainiugan*. Additionally to test the market complexity, the wide range of samples, 71 marketed *Boletus bainiugan* with unknown processing temperatures were selected to be combined with 86 from this study. Table 3 and Fig. 5 present the predictive model parameters for protein, polysaccharide, crude fibers, and fat content based on the different pre-processing methods of FTIR spectroscopy.

The FD-SNV preprocessing method was verified to be a good predictor of protein and polysaccharide content of *Boletus bainiugan*. The optimal model provided $R^2c = 0.926$, RMSEC = 1.315, $R^2p = 0.905$, RMSEP = 1.21, Bias = 0.167 for protein content prediction. The optimal polysaccharide content prediction model $R^2c = 0.831$, RMSEC = 5.373, $R^2p = 0.795$, RMSEP = 4.107, Bias = 0.07 for proteins content prediction. Further, the optimal method for both crude fibers and fats content prediction models was FD-SNV-SG. The model parameters are shown in Table 3 and Fig. 5, Fiber: $R^2c = 0.828$, RMSEC = 0.455, $R^2p = 0.851$, RMSEP = 0.415, Bias = 0.019, Fat: $R^2c = 0.801$, RMSEC = 0.088, $R^2p = 0.85$, RMSEP = 0.077, Bias = 0.007. Reference and prediction plots provide the optimal prediction models for the four nutrient contents, with the calibration set in blue and the prediction set in red (Fig. S6). All sample points are uniformly distributed on both sides of the regression line, and R^2 is close to 1. In conclusion, the proposed FTIR/PLSR model has a reasonable predictive ability and can be applied to the estimation of the nutritional quality of *Boletus bainiugan*.

4. Discussions

The study revolved around differences in the effect of temperature on chemical composition during post-harvest processing of *Boletus bainiugan* and GC-MS, wet chemistry and spectroscopic techniques were chosen to analyze them. This study provides consumers with appropriate drying temperatures to reduce temperature damage to chemical components.

4.1. Differences in VOCs at different temperatures

GC-MS analyses revealed chemical compositional differences between the five drying temperature gradients of *Boletus bainiugan*. PCA and OPLS-DA verified this finding and screened 21 volatile differential metabolites among them. We found 65 °C to be the more favorable temperature for retaining the VOCs in this study. Such as alcohols were significantly higher at 65 °C than at other temperatures. This might be a result of temperature interfering with the interaction of enzymes such as lipoxygenase and hydroperoxide lyase with substrates, leading to inconsistent degradation of unsaturated fatty acids such as linoleic acid (Xiao et al., 2019; Yang et al., 2016). The alcohols 1-Octanol, 3-Octen-1-ol, (Z)- of the C8 backbone structure are the critical alcohols in mushrooms. Increasing temperature decreased the 1-Octanol content, while 3-Octen-1-ol, (Z)- decreased and then increased (Table 4). Also, we enumerate some important alcohols associated with the formation of odour in mushrooms: Benzenemethanol, .alpha.-methyl- (fresh, sweet), Benzenemethanol, 4-methyl- (mild, floral), Cyclohexanol, 1-ethenyl- (tropical, fruity), Cyclohexanol, 3,5-dimethyl- (woody), Cyclooctyl Alcohol (floral), Phenylethyl Alcohol (sweet, apple). None of them reached a maximum content of 75 °C (Table 4). Aldehyde is an essential aroma group and, in mushrooms, is mainly derived from the oxidative degradation of unsaturated fatty acids. The results of this study indicated that 65 °C was the most favorable for Aldehyde production and that a temperature of 75 °C was far too high for the enzyme activity. For example, the (E)-2-Octenal content was significantly higher at 65 °C (0.0107 ± 0.0018 μg/g, $p < 0.05$).

Moreover, the increase in temperature prompted the Maillard reaction affecting the generation of aldehydes, in which benzaldehyde is mainly generated by the Maillard reaction of phenylalanine (Yang et al., 2016). 75 °C (0.0533 ± 0.002 μg/g) resulted in the highest BenzAldehyde content, indicating that this temperature favours the Maillard reaction (Table 4). Nevertheless, 1-Octen-3-one in Ketone has a typical mushroom-like odour, which has a greater impact on the overall aroma. It is primarily obtained by the oxidative degradation of unsaturated fatty acids and the Maillard reaction, and can also be generated by the degradation of ester compounds (Cao et al., 2014; Giri et al., 2010; Liu et al., 2021). 55°C–65 °C favored the retention of Ketone compounds, in agreement with the findings of Wu et al. (2019). Terpenoids were highest at 65 °C, which was significantly different from other temperatures, which is consistent with the findings of (Popa et al., 2022).

4.2. Spectral characterization

FT-NIR and FTIR spectroscopic characterization of chemical information showed differences in the chemical composition of *Boletus bainiugan* at different drying temperatures. For the FT-NIR spectra, the difference between different temperatures is very obvious, with the overall absorption intensity showing 45 °C > 55 °C > 65 °C > 75 °C > 35 °C. In addition, for FTIR is divided into two bands for analysis. The first one is 3600–2500 cm^{-1}, where there are two absorption peaks with a consistent pattern of absorption intensity: 45 °C > 35 °C > 75 °C > 55 °C > 65 °C. The absorption peaks are the same as the absorption peaks of the other two bands. This could be related to carbohydrates, carboxylic acids, amino acids, and carboxylic acids (Lin et al., 2023). This was followed by 1650–400 cm^{-1}, a region with many absorption peaks, with overlap of 35 °C and 45 °C occurring near 1624.25 cm^{-1}, and 55 °C overlapping with 65 °C, which was related to protein content (Table S4). Moreover, the absorption peak intensities of 1399.1, 1027.39, and 525.57 cm^{-1} all showed a consistent pattern: 45 °C > 35 °C > 75 °C > 55 °C > 65 °C.

Overall, the infrared spectra provide a picture of the vibrations of all the chemical constituent groups of the *Boletus bainiugan* substrate as a result of the integrated compositional changes. The results of spectral characterization showed that IR spectra can characterize the effect of drying temperature on the chemical composition of *Boletus bainiugan*.

4.3. Establishment of rapid quality assessment method

The results of nutrient composition showed no significant difference in total protein and crude fiber of *Boletus bainiugan* at different

Table 3
Effectiveness of PLSR model for prediction of total protein, polysaccharide, crude fiber, fat content in *Boletus bainiugan*.

Pretreatment methods	LVs	R^2c	RMSEC	R^2p	RMSEP	Bias
protein						
Origina	18	0.893	1.581	0.837	1.581	0.157
FD-MSC	15	0.921	1.358	0.902	1.261	0.154
FD-SNV	**15**	**0.926**	**1.315**	**0.905**	**1.21**	**0.167**
FD-SNV-SG	15	0.928	1.301	0.907	1.934	0.187
polysaccharide						
Origina	19	0.72	6.91	0.565	5.946	1.075
FD-MSC	19	0.72	7.91	0.565	6.948	1.075
FD-SNV	**19**	**0.831**	**5.373**	**0.795**	**4.107**	**0.070**
FD-SNV-SG	20	0.846	4.66	0.805	4.506	0.636
crude fiber						
Origina	18	0.576	0.734	0.574	0.701	0.024
FD-MSC	20	0.794	0.498	0.818	0.458	0.016
FD-SNV	20	0.805	0.484	0.838	0.432	0.028
FD-SNV-SG	**19**	**0.828**	**0.455**	**0.851**	**0.415**	**0.019**
fat						
Origina	20	0.612	0.124	0.66	0.117	0.007
FD-MSC	20	0.788	0.091	0.841	0.08	0.01
FD-SNV	20	0.797	0.09	0.849	0.078	0.010
FD-SNV-SG	**20**	**0.801**	**0.088**	**0.850**	**0.077**	**0.007**

Note: LVs: latent variables; R^2c: Calibration set coefficient of determination; R^2p: Prediction set coefficient of determination; RMSEC: calibration set root mean square error; RMSEP: prediction set root mean square error; FD: First derivative; MSC: Multiplicative signal correction; SNV: Standard normal variate; SG: Savitzky-Golay.

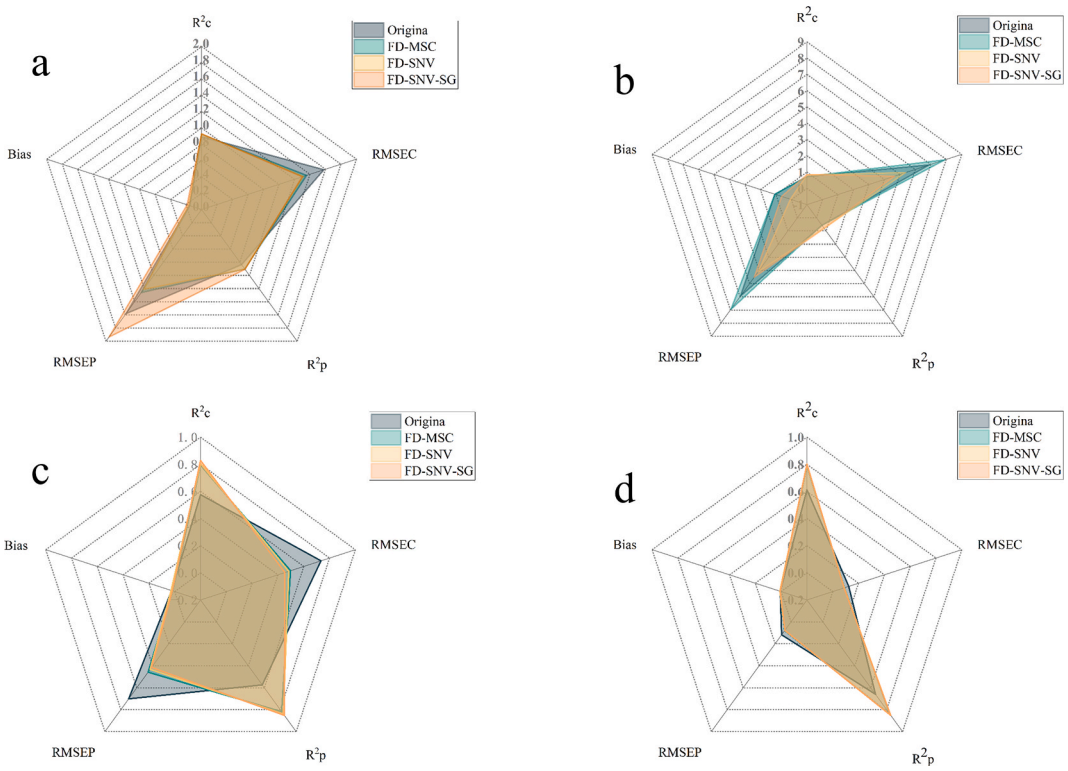

Fig. 5. Performance of PLSR model based on FTIR spectroscopy to predict (a) protein, (b) polysaccharide, (c) crude fiber, and (d) fat content.

Table 4
Differences in the content of important compounds at different temperatures.

Compounds	Content (μg/g)				
	35 °C	45 °C	55 °C	65 °C	75 °C
1-Octanol	0.0081 ± 0.0008a	0.0067 ± 0.0002 ab	0.0063 ± 0.0002b	0.0068 ± 0.0013 ab	0.0063 ± 0.0006b
3-Octen-1-ol, (Z)-	0.0299 ± 0.0049a	0.0211 ± 0.0023b	0.0249 ± 0.0018 ab	0.0267 ± 0.0033 ab	0.0284 ± 0.0025a
4-Hexen-1-ol, acetate	0.0740 ± 0.0188b	0.0595 ± 0.0066b	0.1796 ± 0.0241a	0.1605 ± 0.1122 ab	0.0870 ± 0.0057 ab
Benzenemethanol, .alpha.-methyl-	0.0187 ± 0.0026b	0.0252 ± 0.0022 ab	0.0198 ± 0.0016b	0.0289 ± 0.0065 ab	0.0219 ± 0.0038a
Benzenemethanol, 4-methyl-	0.0131 ± 0.0010a	0.0093 ± 0.0009c	0.0108 ± 0.0016BCE	0.0110 ± 0.0010abc	0.0125 ± 0.0008 ab
Cyclohexanol, 1-ethenyl-	0.4986 ± 0.0383c	0.4122 ± 0.0504c	0.9904 ± 0.1078a	0.8036 ± 0.0660b	0.8598 ± 0.0444b
Cyclohexanol, 3,5-dimethyl-	0.0492 ± 0.0027b	0.0463 ± 0.0062b	0.0871 ± 0.0087a	0.1153 ± 0.0312a	0.0998 ± 0.0169a
Cyclooctyl Alcohol	0.1386 ± 0.0140b	0.2282 ± 0.0230a	0.1337 ± 0.0183b	0.1535 ± 0.0297b	0.1432 ± 0.0179b
Phenylethyl Alcohol	0.3169 ± 0.0657b	0.4265 ± 0.0104a	0.2040 ± 0.0152c	0.2116 ± 0.0083c	0.3105 ± 0.0372b
(E)-2-Octenal	0.0071 ± 0.0008BCE	0.0103 ± 0.0015a	0.0045 ± 0.0021c	0.0107 ± 0.0018a	0.0085 ± 0.0015 ab
BenzAldehyde	0.0450 ± 0.0052c	0.0374 ± 0.0009d	0.0514 ± 0.0018 ab	0.0461 ± 0.0034BCE	0.0533 ± 0.0022a
1-Octen-3-one	0.0312 ± 0.0057a	0.0155 ± 0.0021c	0.0162 ± 0.0005c	0.0119 ± 0.0015c	0.0231 ± 0.0029b

Note: A different superscript letter within a row means a significant difference between the samples ($p < 0.05$).

temperature gradients. Polysaccharides and fat showed higher contents at low temperatures (35 °C, 45 °C and 55 °C) than at high temperatures (65 °C, 75 °C). This indicates that elevated temperatures are detrimental to the retention of crude total polysaccharides and fats. Elevated temperatures will favor Maillard reactions, which will reduce protein retention (Xu et al., 2019). This is consistent with our results (Table S4). 65 °C had the lowest fatty acid content (1.52 ± 0.18 g/100g) which is in agreement with the findings of Oancea et al. (2023). The total polysaccharide content showed an increasing and then decreasing trend with increasing temperature, and was highest at 55 °C. Previous studies have shown that the polysaccharide content tends to increase during the drying process at 50–70 °C, after which the content decreases significantly with increasing temperature (Guo et al., 2021). This inconsistency in the results could be because we used a blast-drying oven. Also crude fibre content was the difference was not significant.

Furthermore, we established a fitting relationship between FTIR and the composition of nutrient with R^2p in the range of 0.795–0.905 and Bias in the range of 0.007–0.167, ensuring predictive reliability. Our model performance is superior to others (Andersen et al., 2023). R^2p in this study achieved similar results with the study of Tian et al. (2021) and the results are plausible. However, more studies are needed to improve the accuracy of the model before practical application.

This study provides insight into the effect of different drying temperatures on VOCs and nutrient content of dried white bovine mushrooms. It was found that 65 °C was most favorable for the retention of VOCs. The contents of total protein, fat, polysaccharide, and fiber were highly correlated with the FTIR spectra. Of course, various other factors affect the nutritional quality of *Boletus bainiugan*, such as origin, species, preservation conditions, storage age, etc., and should be taken into account simultaneously in future studies.

5. Conclusion

In summary, the present study characterizes the chemical

composition of *Boletus bainiugan* based on GC-MS, wet chemistry, and IR spectroscopy techniques at different drying temperatures. A new method based on IR spectroscopy and chemometrics was developed to reliably analyze the chemical constituents of *Boletus bainiugan* under processing. The results of the GC-MS analyses revealed that 65 °C retained a high level of volatile constituent substances. There was variability in volatile substances at different drying temperatures, and 21 differential metabolites were screened by OPLS-DA. Simultaneously, the nutrient composition of *Boletus bainiugan* at different drying temperatures was determined and found to be lower at 55 °C and 65 °C. Then the presence of differences in the chemical composition of *Boletus bainiugan* at different temperatures was characterized by FT-NIR and FTIR spectroscopy. The chemometrics model effectively identifies differences in chemical composition, and predicts protein, polysaccharide, crude fiber, and fat content of *Boletus bainiugan* at different temperatures.

CRediT authorship contribution statement

Chuanmao Zheng: Conceptualization, Data organization, Software, Visualization, Writing-original manuscript, Writing – review & editing. **Jieqing Li:** Conceptualization, Data curation, Validation. **Honggao Liu:** Conceptualization, Formal analysis, Project administration. **Yuanzhong Wang:** Methodology, Project administration, Resources, All the authors approved the final version of the manuscript.

Declaration of competing interest

The authors declare no competing interests.

Data availability

The data that has been used is confidential.

Acknowledgments

This work was supported by National Natural Science Foundation of China [Grant Number: 32160735]; General Program Project of Joint Special Project on Basic Agricultural Research in Yunnan Province [Grant Number: 202301BD070001-167]; Special Program for the Major Science and Technology Projects of Yunnan Province [Grant Number: 202202AE090001].

Appendix A. Supplementary data

Supplementary data to this article can be found online at https://doi.org/10.1016/j.crfs.2024.100819.

References

Andersen, P.V., Afseth, N.K., Aaby, K., Gaarder, M.Ø., Remberg, S.F., Wold, J.P., 2023. Prediction of chemical and sensory properties in strawberries using Raman spectroscopy. Postharvest Biol. Technol. 201, 112370 https://doi.org/10.1016/j.postharvbio.2023.112370.

Archibald, R.M., Frame, E.G., Senesky, D., 1958. Nitrogen by the Kjeldahl method. In: Standard Methods of Clinical Chemistry, 2. Elsevier, pp. 91–99. https://doi.org/10.1016/B978-1-4831-9683-1.50016-2.

Aykas, D.P., Sinir, G.O., Borba, K.R., 2023. Determination of quality traits and possible adulteration of molasses using FT-IR spectroscopy: a study from Turkish market. Food Chem. 427, 136727 https://doi.org/10.1016/j.foodchem.2023.136727.

Badaró, A.T., Hebling E Tavares, J.P., Blasco, J., Aleixos-Borrás, N., Barbin, D.F., 2022. Near infrared techniques applied to analysis of wheat-based products: recent advances and future trends. Food Control 140, 109115. https://doi.org/10.1016/j.foodcont.2022.109115.

Cao, J., Zou, X.-G., Deng, L., Fan, Y.-W., Li, H., Li, J., Deng, Z.-Y., 2014. Analysis of nonpolar lipophilic aldehydes/ketones in oxidized edible oils using HPLC-QqQ-MS for the evaluation of their parent fatty acids. Food Res. Int. 64, 901–907. https://doi.org/10.1016/j.foodres.2014.08.042.

Chen, Y., Huang, J., Yeap, Z.Q., Zhang, X., Wu, S., Ng, C.H., Yam, M.F., 2018. Rapid authentication and identification of different types of A. roxburghii by Tri-step FT-IR spectroscopy. Spectrochim. Acta Mol. Biomol. Spectrosc. 199, 271–282. https://doi.org/10.1016/j.saa.2018.03.061.

Chen, Y., Zhang, R., Song, Y., He, J., Sun, J., Bai, J., An, Z., Dong, L., Zhan, Q., Abliz, Z., 2009. RRLC-MS/MS-based metabonomics combined with in-depth analysis of metabolic correlation network: finding potential biomarkers for breast cancer. Analyst 134 (10), 2003. https://doi.org/10.1039/b907243h.

Choong, Y.K., Sun, S.-Q., Zhou, Q., Ismail, Z., Rashid, B.A.A., Tao, J.-X., 2011. Determination of storage stability of the crude extracts of *Ganoderma lucidum* using FTIR and 2D-IR spectroscopy. Vib. Spectrosc. https://doi.org/10.1016/j.vibspec.2011.05.008. S0924203111000774.

Christou, C., Agapiou, A., Kokkinofta, R., 2018. Use of FTIR spectroscopy and chemometrics for the classification of carobs origin. J. Adv. Res. 10, 1–8. https://doi.org/10.1016/j.jare.2017.12.001.

Cruz-Tirado, J.P., Vieira, M.S.D.S., Amigo, J.M., Siche, R., Barbin, D.F., 2023. Prediction of protein and lipid content in black soldier fly (*Hermetia illucens* L.) larvae flour using portable NIR spectrometers and chemometrics. Food Control 153, 109969. https://doi.org/10.1016/j.foodcont.2023.109969.

Deng, G., Li, J., Liu, H., Wang, Y., 2023. Volatile compounds and aroma characteristics of mushrooms: a review. Crit. Rev. Food Sci. Nutr. 1–18. https://doi.org/10.1080/10408398.2023.2261133.

Dong, J.-E., Zhang, S., Li, T., Wang, Y.-Z., 2022. 2DCOS combined with CNN and blockchain to trace the species of boletes. Microchem. J. 177, 107260 https://doi.org/10.1016/j.microc.2022.107260.

Drees, A., Brockelt, J., Cvancar, L., Fischer, M., 2023. Rapid determination of the shell content in cocoa products using FT-NIR spectroscopy and chemometrics. Talanta 256, 124310. https://doi.org/10.1016/j.talanta.2023.124310.

Esteves, C.S.M., de Redrojo, E.M.M., Luis García Manjón, J., Moreno, G., Antunes, F.E., Montalvo, G., Ortega-Ojeda, F.E., 2022. Combining FTIR-ATR and OPLS-DA methods for magic mushrooms discrimination. Forensic Chemistry 29, 100421. https://doi.org/10.1016/j.forc.2022.100421.

Gan, Y., Yang, T., Gu, W., Guo, L., Qiu, R., Wang, S., Zhang, Y., Tang, M., Yang, Z., 2024. Using HS-GC-MS and flash GC e-nose in combination with chemometric analysis and machine learning algorithms to identify the varieties, geographical origins and production modes of *Atractylodes lancea*. Ind. Crop. Prod. 209, 117955 https://doi.org/10.1016/j.indcrop.2023.117955.

Giri, A., Osako, K., Ohshima, T., 2010. Identification and characterisation of headspace volatiles of fish *miso*, a Japanese fish meat based fermented paste, with special emphasis on effect of fish species and meat washing. Food Chem. 120 (2), 621–631. https://doi.org/10.1016/j.foodchem.2009.10.036.

Guo, L., Lan, N., Li, H., Xiang, P., Kan, H., 2021. Effect of hot air drying temperature on the quality and antioxidant activity of *Boletus edulis* Bull.: Fr. J. Food Process. Preserv. 45 (6) https://doi.org/10.1111/jfpp.15540.

He, G., Yang, S., Wang, Y., 2023. An integrated chemical characterization based on FT-NIR, and GC–MS for the comparative metabolite profiling of 3 species of the genus Amomum. Anal. Chim. Acta 1280, 341869. https://doi.org/10.1016/j.aca.2023.341869.

Jingying, C., Baocai, L., Ying, C., Wujun, Z., Yunqing, Z., Yingzhen, H., Yin Tew, W., Shun Ong, P., Seng Yan, C., Wei Loh, H., Fei Yam, M., 2023. Discrimination of *Dioscorea* species (Chinese yam) using FT-IR integrated with chemometric approach. Spectrochim. Acta Mol. Biomol. Spectrosc., 123229 https://doi.org/10.1016/j.saa.2023.123229.

Kushairi, N., Tarmizi, N.A.K.A., Phan, C.W., Macreadie, I., Sabaratnam, V., Naidu, M., David, P., 2020. Modulation of neuroinflammatory pathways by medicinal mushrooms, with particular relevance to Alzheimer's disease. Trends Food Sci. Technol. 104, 153–162. https://doi.org/10.1016/j.tifs.2020.07.029.

Lin, X.-W., Liu, R., Wang, S., Yang, J.-W., Tao, N.-P., Wang, X.-C., Zhou, Q., Xu, C.-H., 2023. Direct identification and quantitation of protein peptide powders based on multi-molecular infrared spectroscopy and multivariate data fusion. J. Agric. Food Chem. 71 (28), 10819–10829. https://doi.org/10.1021/acs.jafc.3c01841.

Liu, Q., Cui, X., Song, Z., Kong, W., Kang, Y., Kong, W., Ng, T.B., 2021. Coating shiitake mushrooms (*Lentinus edodes*) with a polysaccharide from Oudemansiella radicata improves product quality and flavor during postharvest storage. Food Chem. 352, 129357 https://doi.org/10.1016/j.foodchem.2021.129357.

Lu, X., Hou, H., Fang, D., Hu, Q., Chen, J., Zhao, L., 2022. Identification and characterization of volatile compounds in *Lentinula edodes* during vacuum freeze-drying. J. Food Biochem. 46 (6) https://doi.org/10.1111/jfbc.13814.

Ma, X., Li, C., Huang, R., Zhang, K., Wang, Q., Fu, C., Liu, W., Sun, C., Wang, P., Wang, F., Deng, X., 2021. Rice brittle Culm19 encoding cellulose synthase subunit CESA4 causes dominant brittle phenotype but has No distinct influence on growth and grain yield. Rice 14 (1), 95. https://doi.org/10.1186/s12284-021-00536-2.

Mabasa, X.E., Mathomu, L.M., Madala, N.E., Musie, E.M., Sigidi, M.T., 2021. Molecular spectroscopic (FTIR and UV-vis) and hyphenated chromatographic (UHPLC-qTOF-MS) analysis and *in vitro* bioactivities of the *Momordica balsamina* leaf extract. Biochemistry Research International 2021, 1–12. https://doi.org/10.1155/2021/2854217.

Moţ, A.C., Silaghi-Dumitrescu, R., Sârbu, C., 2011. Rapid and effective evaluation of the antioxidant capacity of propolis extracts using DPPH bleaching kinetic profiles, FT-IR and UV–vis spectroscopic data. J. Food Compos. Anal. 24 (4–5), 516–522. https://doi.org/10.1016/j.jfca.2010.11.006.

Nielsen, S.S., Carpenter, C., 2017. Fat content determination. In: Nielsen, S.S. (Ed.), Food Analysis Laboratory Manual. Springer International Publishing, pp. 121–129. https://doi.org/10.1007/978-3-319-44127-6_12.

Oancea, S., Popa, M., Socaci, S.A., Dulf, F.V., 2023. Comparative study of raw and dehydrated *Boletus edulis* mushrooms by hot air and centrifugal vacuum processes: functional properties and fatty acid and aroma profiles. Appl. Sci. 13 (6), 3630. https://doi.org/10.3390/app13063630.

Peng, D., Zhou, Q., Su, M., Zheng, S., Xie, S., Li, J., 2024. Quantitative determination of the carbonyl value in frying oils based on LF-NMR combined with chemometrics. Lebensm. Wiss. Technol. 198, 116067 https://doi.org/10.1016/j.lwt.2024.116067.

Popa, M., Tăuşan, I., Drăghici, O., Soare, A., Oancea, S., 2022. Influence of convective and vacuum-type drying on quality, microstructural, antioxidant and thermal properties of pretreated *Boletus edulis* mushrooms. Molecules 27 (13), 4063. https://doi.org/10.3390/molecules27134063.

Rohman, A., Man, Y.B.C., 2010. Fourier transform infrared (FTIR) spectroscopy for analysis of extra virgin olive oil adulterated with palm oil. Food Res. Int. 43 (3), 886–892. https://doi.org/10.1016/j.foodres.2009.12.006.

Sun, X., Wang, Z., Li, X., Du, S., Lin, D., Shao, Y., 2023. Effects of *Yucca schidigera* extract on serum biochemical parameters, humoral immune response, and intestinal health in young pigeons. Front. Vet. Sci. 9, 1077555 https://doi.org/10.3389/fvets.2022.1077555.

Surek, M., Cobre, A.D.F., Fachi, M.M., Santos, T.G., Pontarolo, R., Crisma, A.R., Felipe, K. B., Souza, W.M.D., 2022. Propolis authentication of stingless bees by mid-infrared spectroscopy and chemometric analysis. Lebensm. Wiss. Technol. 161, 113370 https://doi.org/10.1016/j.lwt.2022.113370.

Tian, R., Liang, Z.-Q., Wang, Y., Zeng, N.-K., 2022. Analysis of aromatic components of two edible mushrooms, *Phlebopus portentosus* and *Cantharellus yunnanensis* using HS-SPME/GC-MS. Results in Chemistry 4, 100282. https://doi.org/10.1016/j.rechem.2022.100282.

Tian, W., Chen, G., Zhang, G., Wang, D., Tilley, M., Li, Y., 2021. Rapid determination of total phenolic content of whole wheat flour using near-infrared spectroscopy and chemometrics. Food Chem. 344, 128633 https://doi.org/10.1016/j.foodchem.2020.128633.

Vanitha, A., Kalimuthu, K., Chinnadurai, V., Nisha, K.M.J., 2019. Phytochemical screening, FTIR and GCMS analysis of aqueous extract of *Caralluma bicolor*–An endangered plant. Asian J. Pharm. Pharmacol. 5 (6), 1122–1130. https://doi.org/10.31024/ajpp.2019.5.6.7.

Veselá, A., Barros, A.S., Synytsya, A., Delgadillo, I., Čopíková, J., Coimbra, M.A., 2007. Infrared spectroscopy and outer product analysis for quantification of fat, nitrogen, and moisture of cocoa powder. Anal. Chim. Acta 601 (1), 77–86. https://doi.org/10.1016/j.aca.2007.08.039.

Wu, X., Zhang, M., Bhandari, B., 2019. A novel infrared freeze drying (IRFD) technology to lower the energy consumption and keep the quality of Cordyceps militaris. Innovat. Food Sci. Emerg. Technol. 54, 34–42. https://doi.org/10.1016/j.ifset.2019.03.003.

Xiao, Z., Xiang, P., Zhu, J., Zhu, Q., Liu, Y., Niu, Y., 2019. Evaluation of the perceptual interaction among sulfur compounds in mango by feller's additive model, odor activity value, and vector model. J. Agric. Food Chem. 67 (32), 8926–8937. https://doi.org/10.1021/acs.jafc.9b03156.

Xie, J., Wang, L., Deng, Y., Yuan, H., Zhu, J., Jiang, Y., Yang, Y., 2023. Characterization of the key odorants in floral aroma green tea based on GC-E-Nose, GC-IMS, GC-MS and aroma recombination and investigation of the dynamic changes and aroma formation during processing. Food Chem. 427, 136641 https://doi.org/10.1016/j.foodchem.2023.136641.

Xu, L., Fang, X., Wu, W., Chen, H., Mu, H., Gao, H., 2019. Effects of high-temperature pre-drying on the quality of air-dried shiitake mushrooms (*Lentinula edodes*). Food Chem. 285, 406–413. https://doi.org/10.1016/j.foodchem.2019.01.179.

Yan, Z., Liu, H., Li, J., Wang, Y., 2023. Qualitative and quantitative analysis of *Lanmaoa asiatica* in different storage years based on FT-NIR combined with chemometrics. Microchem. J. 189, 108580 https://doi.org/10.1016/j.microc.2023.108580.

Yang, W., Yu, J., Pei, F., Mariga, A.M., Ma, N., Fang, Y., Hu, Q., 2016. Effect of hot air drying on volatile compounds of Flammulina velutipes detected by HS-SPME–GC–MS and electronic nose. Food Chem. 196, 860–866. https://doi.org/10.1016/j.foodchem.2015.09.097.

Ye, Y., Zheng, S., Wang, Y., 2024. Analysis of aroma components changes in Gannan navel orange at different growth stages by HS-SPME-GC–MS, OAV, and multivariate analysis. Food Res. Int. 175, 113622 https://doi.org/10.1016/j.foodres.2023.113622.

Zhang, J., Yu, H., Li, S., Zhong, X., Wang, H., Liu, X., 2020. Comparative metabolic profiling of *Ophiocordyceps sinensis* and its cultured mycelia using GC–MS. Food Res. Int. 134, 109241 https://doi.org/10.1016/j.foodres.2020.109241.

Zhang, K., Pu, Y.-Y., Sun, D.-W., 2018. Recent advances in quality preservation of postharvest mushrooms (*Agaricus bisporus*): a review. Trends Food Sci. Technol. 78, 72–82. https://doi.org/10.1016/j.tifs.2018.05.012.

Zhang, Y., Wang, Y., 2023a. Machine learning applications for multi-source data of edible crops: a review of current trends and future prospects. Food Chem. X 19, 100860. https://doi.org/10.1016/j.fochx.2023.100860.

Zhang, Y., Wang, Y., 2023b. Recent trends of machine learning applied to multi-source data of medicinal plants. Journal of Pharmaceutical Analysis. https://doi.org/10.1016/j.jpha.2023.07.012. S2095177923001612.

Zheng, C., Li, J., Liu, H., Wang, Y., 2023a. Data fusion of FT-NIR and ATR-FTIR spectra for accurate authentication of geographical indications for *Gastrodia elata* Blume. Food Biosci. 56, 103308 https://doi.org/10.1016/j.fbio.2023.103308.

Zheng, C., Li, J., Liu, H., Wang, Y., 2023b. Review of postharvest processing of edible wild-grown mushrooms. Food Res. Int. 173, 113223 https://doi.org/10.1016/j.foodres.2023.113223.

Zheng, Q., Li, X., Liu, T., Zhang, Y., Liu, J., Zhang, H., Li, W., Gao, X., 2021. Effects of air-impingement jet drying on drying kinetics, color, polyphenol compounds, and antioxidant activities of *Boletus aereus* slices. J. Food Sci. 86 (5), 2131–2144. https://doi.org/10.1111/1750-3841.15702.

Zhong, L., Zou, X., Wu, S., Chen, L., Fang, S., Zhong, W., Xie, L., Zhan, R., Chen, L., 2024. Volatilome and flavor analyses based on e-nose combined with HS-GC-MS provide new insights into ploidy germplasm diversity in Platostoma palustre. Food Res. Int. 183, 114180 https://doi.org/10.1016/j.foodres.2024.114180.